Global Biogeochemical Cycles®

AGU ADVANCING EARTH AND SPACE SCIENCE

RESEARCH ARTICLE
10.1029/2021GB007018

Special Section:
Understanding carbon-climate feedbacks

Quantifying the Role of Seasonality in the Marine Carbon Cycle Feedback: An ESM2M Case Study

Andrea J. Fassbender[1,2], Sarah Schlunegger[3], Keith B. Rodgers[4,5], and John P. Dunne[6]

[1]Monterey Bay Aquarium Research Institute, Moss Landing, CA, USA, [2]Now at NOAA/OAR Pacific Marine Environmental Laboratory, Seattle, WA, USA, [3]Program in Atmospheric and Oceanic Sciences, Princeton University, Princeton, NJ, USA, [4]Center for Climate Physics, Institute for Basic Science, Busan, South Korea, [5]Pusan National University, Busan, South Korea, [6]NOAA/OAR Geophysical Fluid Dynamics Laboratory, Princeton, NJ, USA

Key Points:

- Ocean anthropogenic carbon (C_{ant}) accumulation enhances the sensitivity of ocean carbon dioxide partial pressure (pCO_2) to seasonal changes in ocean physics and biology
- C_{ant}-induced changes in the pCO_2 seasonal cycle under RCP8.5 forcing increase cumulative ocean carbon uptake by 8% in ESM2M
- The net increase in cumulative ocean carbon uptake is driven by the interaction of wintertime changes in pCO_2 and strong winter winds

Supporting Information:

Supporting Information may be found in the online version of this article.

Correspondence to:

A. J. Fassbender,
andrea.j.fassbender@noaa.gov

Citation:

Fassbender, A. J., Schlunegger, S., Rodgers, K. B., & Dunne, J. P. (2022). Quantifying the role of seasonality in the marine carbon cycle feedback: An ESM2M case study. *Global Biogeochemical Cycles*, *36*, e2021GB007018. https://doi.org/10.1029/2021GB007018

Received 25 MAR 2021
Accepted 20 MAY 2022

Abstract Observations and climate models indicate that changes in the seasonal amplitude of sea surface carbon dioxide partial pressure (A-pCO_2) are underway and driven primarily by anthropogenic carbon (C_{ant}) accumulation in the ocean. This occurs because pCO_2 is more responsive to seasonal changes in physics (including warming) and biology in an ocean that contains more C_{ant}. A-pCO_2 changes have the potential to alter annual ocean carbon uptake and contribute to the overall marine carbon cycle feedback. Using the GFDL ESM2M Large Ensemble and a novel analysis framework, we quantify the influence of C_{ant} accumulation on pCO_2 seasonal cycles and sea-air CO_2 fluxes. Specifically, we reconstruct alternative evolutions of the contemporary ocean state in which the *sensitivity* of pCO_2 to seasonal thermal and biophysical variation is fixed at preindustrial levels, however the background, mean-state pCO_2 fully responds to anthropogenic forcing. We find near-global A-pCO_2 increases of >100% by 2100, under RCP8.5 forcing, with rising C_{ant} accounting for ~100% of thermal and ~50% of nonthermal pCO_2 component amplitude changes. The other ~50% of nonthermal pCO_2 component changes are attributed to modeled changes in ocean physics and biology caused by climate change. C_{ant}-induced A-pCO_2 changes cause an 8.1 ± 0.4% (ensemble mean ± 1σ) *increase* in ocean carbon uptake by 2100. This is because greater wintertime wind speeds enhance the impact of wintertime pCO_2 changes, which work to increase the ocean carbon sink. Thus, the seasonal ocean carbon cycle feedback works in opposition to the larger, mean-state feedback that *reduces* ocean carbon uptake by ~60%.

Plain Language Summary Using simulations of an Earth System Model, we isolate different factors contributing to future changes in the surface ocean carbon dioxide partial pressure (pCO_2). We examine how the seasonal cycle of pCO_2, and the associated sea-air exchange of CO_2, responds to changes in the ocean's temperature, circulation, biology, and chemistry. We find that the pCO_2 seasonal cycle is significantly amplified across the global ocean (by ~100% on average). This occurs because pCO_2 is more responsive to seasonal changes in temperature as well as biological and physical (biophysical) processes in a future ocean that contains more anthropogenic carbon (C_{ant}). The increased temperature sensitivity is almost exclusively due to added C_{ant}. The increased biophysical sensitivity is equally due to added C_{ant} and changes in ocean physics and biology caused by climate change. Seasonal wind speed variation systematically enhances the impact of altered pCO_2 seasonal cycles during wintertime, causing an 8% increase in the ocean carbon sink strength by the year 2100. Within the evaluated model, this indicates that the seasonal ocean carbon cycle feedback works in opposition to the larger, mean-state ocean carbon cycle feedback, which may cause up to a ~60% reduction in the ocean sink by the year 2100.

1. Introduction

The flux of carbon dioxide gas (CO_2) across the air-sea interface is the primary mechanism by which anthropogenic carbon (C_{ant}) enters the ocean, which presently stores a C_{ant} inventory equivalent to ~40% of the fossil carbon emitted since the preindustrial period (Friedlingstein et al., 2020; Gruber et al., 2019; Khatiwala et al., 2013). Over time, the accumulation of C_{ant} in the ocean will reduce the efficiency of further C_{ant} uptake (Broecker et al., 1979; Revelle & Suess, 1957; Sundquist et al., 1979), representing an important and time-sensitive feedback in the climate system (Archer et al., 2009; Katavouta et al., 2018; Rodgers et al., 2020). This positive (i.e., climate-change enhancing) carbon cycle feedback is caused by a decline the chemical buffering capacity of seawater as the upper ocean hydrogen ion concentration increases and the carbonate ion concentration decreases with continued C_{ant} accumulation (Egleston et al., 2010; Fassbender et al., 2017; Orr et al., 2005).

Rodgers et al. (2020) recently estimated that this erosion of efficiency could reduce ocean carbon uptake by up to ~60% in the historical-RCP8.5 scenario (1850–2100; Figure 2c in their paper). Even so, the ocean is expected to remain the dominant C_{ant} sink on century to millennial timescales due to ocean overturning as well as long-term augmentation of the ocean buffering capacity through chemical weathering, a negative climate feedback process (Archer, 2005; Archer et al., 1997). Less clear is the individual role of short-term (i.e., seasonal) physical, chemical, and biological mechanisms that drive changes in transient ocean carbon uptake efficiency.

The sea-air flux of CO_2 is driven by the gradient between the oceanic and atmospheric partial pressure of CO_2 ($\Delta pCO_{2\ Sea\text{-}Air}$). Since atmospheric CO_2 is relatively well mixed, regional differences in $\Delta pCO_{2\ Sea\text{-}Air}$ are primarily controlled by variability in sea surface pCO_2, which is driven by the temperature-, salinity-, and pressure-dependent solubility of CO_2 (Weiss, 1974) as well as the biological and physical processes (such as net primary production and ocean mixing) that modify surface ocean carbonate chemistry (Takahashi et al., 2002). Throughout much of the open ocean, the largest surface variations in pCO_2 occur on seasonal timescales, driven by the concurrent, and often competing, influences of biological and physical (or biophysical) processes with temperature (Takahashi et al., 1993, 2002). Rising ocean carbon content provides additional chemical leverage to these drivers, allowing the same mechanisms to exert a greater influence on pCO_2 (Riebesell et al., 2009).

Recently, a near global amplification of seasonal pCO_2 extremes (2.2 ± 0.4 µatm per decade) was identified in a ~30-year observational data product (Landschützer et al., 2018). The potential implications for marine ecosystems exposed to larger seasonal pCO_2 ranges are extensive, including greater likelihood of seasonal hypercapnic conditions (McNeil & Sasse, 2016) and physiological acidosis (Pörtner, 2008) caused by accompanying amplification (~80%) of the hydrogen ion concentration seasonal cycle (Kwiatkowski & Orr, 2018). Further, theoretical and modeling work has suggested that asymmetries in seasonal cycle changes could alter the net annual ocean carbon uptake (Fassbender et al., 2018; Gorgues et al., 2010; Hauck et al., 2015; Hauck & Völker, 2015; Rodgers et al., 2008). For example, if increases in the seasonal pCO_2 high and decreases in the seasonal pCO_2 low do not lead to compensating seasonal sea-air flux changes, the net annual carbon sink strength will be altered. Such changes in the ocean sink strength would contribute a seasonal component to the overall marine carbon cycle feedback, which has not yet been considered under established and emerging feedback frameworks (Arora et al., 2013; Friedlingstein et al., 2003; Goodwin et al., 2019; Katavouta et al., 2018; Schwinger et al., 2014).

Here we introduce an offline method for quantifying how sea surface pCO_2 and sea-air CO_2 fluxes are impacted by rising surface ocean carbon content. Our aim is to characterize how C_{ant} accumulation directly influences the efficacy at which thermal, physical, and biological drivers modulate pCO_2 to gain insight about the processes responsible for changes in the magnitude, structure, and phasing of the pCO_2 seasonal cycle and resulting sea-air CO_2 flux. A key challenge in determining how pCO_2 seasonal cycle modulations contribute to climate feedbacks is identifying a neutral state against which the feedback can be evaluated. In other words, rather than simply looking at amplitude changes about the annual mean, the question is whether asymmetries in seasonal extrema changes can lead to altered annual net fluxes. Answering this question requires isolating the explicit impact of C_{ant} on seasonal drivers of pCO_2 variation, which has motivated us to develop this alternative feedback framework.

2. Description of Model Data and Carbonate System Calculations

We use output from the Geophysical Fluid Dynamics Laboratory (GFDL) ESM2M Large Ensemble (30 members; Rodgers et al., 2015), which includes the full suite of ocean biogeochemical parameters saved at a monthly resolution, to evaluate the historical-RCP8.5 period (1950–2100). All model output fields are publicly available and can be accessed at poseidon.princeton.edu. We test our offline methodology using a high-CO_2-concentration pathway scenario (RCP8.5) to determine whether a seasonal CO_2 flux feedback and the mechanisms driving it are detectable and quantifiable. Using the ESM2M Large Ensemble allows us to characterize the robustness of our methodology to the presence of internal climate variability, and thereby applicability of the method to individual Earth System Model simulations.

ESM2M pCO_2 values and sea-air CO_2 fluxes have been assessed previously and exhibit average performance in reproducing the modern mean state and seasonality (Gallego et al., 2018; Goris et al., 2018; Mongwe et al., 2018; Pilcher et al., 2015). For example, Pilcher et al. (2015) performed an analysis of 18 CMIP5 models and found that the GFDL models, including ESM2M, exhibited elevated performance in reproducing the observed pCO_2 seasonal cycles (amplitude and phasing) and annual mean values for five generalized latitudinal domains of

the global surface ocean. Importantly, Pilcher et al. (2015) found that the GFDL models performed particularly well in the subpolar seasonally stratified biome regions where models tend to disagree most on the seasonal cycle amplitude and phasing for both pCO_2 (Gallego et al., 2018; Goris et al., 2018) and CO_2 flux (Mongwe et al., 2018; Nevison et al., 2016).

All model variables used were first re-gridded to a 1° × 1° horizontal scale using the flux-conservative coupler algorithms from ESM2M prior to making offline calculations. Carbonate system calculations were performed using the MATLAB program CO2SYS version 1.1 (Lewis & Wallace, 1998; van Heuven et al., 2011). Following the approach used for ESM2M, we apply the carbonate system dissociation constants of Mehrbach et al. (1973) as refitted by Dickson and Millero (1987), the hydrogen sulfate dissociation constant of Dickson et al. (1990), and the boron-to-chlorinity ratio of Uppström (1974). Offline carbonate chemistry computations using the re-gridded monthly data required a preliminary step of calculating dissolved inorganic carbon (DIC) from other ESM2M parameters to enforce internal carbonate system consistency. Further documentation of our methodology is included in the Supporting Information S1 (Text S1, Figure S1).

3. Methodology

3.1. Overview

To quantify how C_{ant} accumulation influences the efficacy at which thermal, physical, and biological drivers modulate surface ocean pCO_2 seasonally, we reconstruct transient model pCO_2 values while keeping the *sensitivity* of pCO_2 to seasonal variations in temperature, DIC, and total alkalinity (TA) fixed at preindustrial levels. We allow the underlaying mean-state temperature, DIC, TA, and pCO_2 to evolve with anthropogenic forcing; however, by fixing the *sensitivity* of pCO_2 to seasonal variations in the drivers at pre-industrial levels, we remove the impact that C_{ant} accumulation has upon seasonal pCO_2 variations. This allows us to disentangle pCO_2 seasonal cycle alterations caused directly by C_{ant} accumulation (i.e., chemical leverage) versus those caused by changes in ocean physics (including warming) and biology resulting from climate change. As there is no analog metric in established feedback frameworks, we use the symbol Ø to signify when anthropogenic chemical leverage has been removed from the seasonal cycle drivers.

3.2. Annual Mean pCO_2 Reference Value

Our offline methodology requires a transient reference value for the annual mean pCO_2 from which to assess the seasonal variations during each model year. Defining this reference must be done with nuance, as we aim to resolve asymmetric changes in the pCO_2 seasonal cycle, which would be obscured by direct averaging. To define the annual mean pCO_2 reference value, we compute pCO_2 from the annual mean values of pCO_2's constituent drivers: DIC, TA, temperature, salinity, and nutrients. This yields the pCO_2 annual mean value that would result if the sensitivity of pCO_2 to the drivers was linear across the seasonal cycle. This provides a more "neutral" estimate of the annual mean that is less influenced by the seasonal extrema we seek to identify (Figure S2 in Supporting Information S1). We use this indirect approach to compute annual mean pCO_2 values for both the preindustrial and transient periods and apply the subscript "AM" as a reminder of this methodological nuance (e.g., $pCO_{2\ AM}$; Figures 1a and 1d).

3.3. Thermal and Biophysical pCO_2 Components

Seasonal variation in pCO_2 can be conceptualized as arising from two distinct drivers, thermal (T) and biophysical (BP), that work concurrently to yield pCO_2 seasonality that varies by region. For example, modern pCO_2 values generally peak during summer in the subtropical gyres due to prevailing thermal influence and during winter in the high latitudes due to prevailing biophysical influence (Takahashi et al., 2002). Over the 1950 to 2100 historical-RCP8.5 period, we expect the invasion flux of C_{ant} into the ocean not only to cause sea surface pCO_2 values to rise and CO_2 buffering capacity to fall, but also to increase the sensitivity of pCO_2 to seasonal temperature and biophysical variations (Fassbender et al., 2018; Landschützer et al., 2018; Riebesell et al., 2009).

To remove the influence of C_{ant}-induced sensitivity changes (i.e., chemical leverage) on the thermal pCO_2 component, we calculate the monthly pCO_2 values, for each simulation year and grid, using annual mean salinity, DIC, phosphate, and silicate values with monthly temperature values and the preindustrial (PI) period climatological

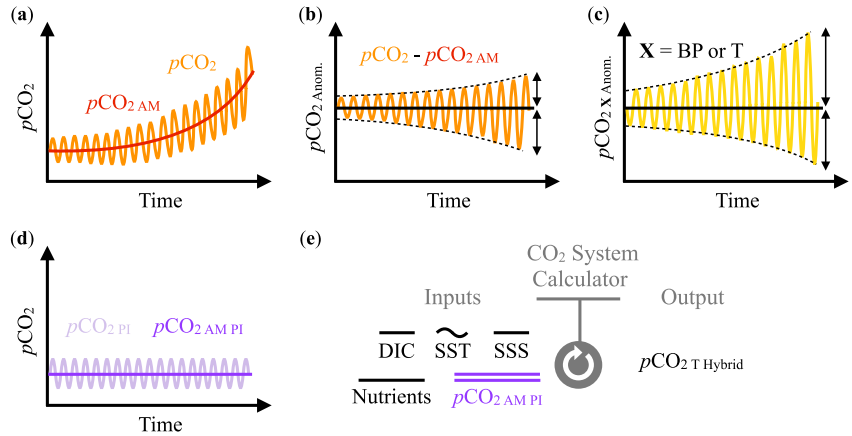

Figure 1. Schematic of some key methodological steps. (a) For each model year and grid, annual carbon dioxide partial pressure (pCO_2) reference values ($pCO_{2\,AM}$) are computed from annually averaged (signified by overbars) sea surface $\overline{DIC}$, $\overline{TA}$, temperature ($\overline{SST}$), salinity ($\overline{SSS}$), and nutrient values using a CO_2 system calculator. (b) This approach (rather than directly averaging monthly pCO_2 values from a given year) makes it possible to identify seasonally asymmetric changes in monthly pCO_2 anomalies (Anom.). (c) Thermal and nonthermal processes that impact pCO_2 work concurrently and often in opposition such that their associated monthly pCO_2 anomalies ($pCO_{2\,T\,Anom.}$ and $pCO_{2\,BP\,Anom.}$) are generally much larger than the net $pCO_{2\,Anom.}$ values. (d) Using the same approach, annual pCO_2 reference values are computed for the preindustrial (PI) period ($pCO_{2\,AM\,PI}$). (e) A climatology of these annual reference values over the 240-year PI period ($\overline{pCO_{2\,AM\,PI}}$) is used to compute $pCO_{2\,T\,Hybrid}$. $\overline{pCO_{2\,AM\,PI}}$ is then subtracted from $pCO_{2\,T\,Hybrid}$ (not shown) to isolate the thermal pCO_2 component monthly anomalies that would result if the sensitivity of pCO_2 to seasonal SST variation ($\widetilde{SST}$) were held at PI levels ($\Delta pCO_{2\,T\,\emptyset\,Anom.}$; Equation 1).

annual mean pCO_2 value ($\overline{\overline{pCO_{2\,AM\,PI}}}$; Figure 1e). Since each 1°C change in temperature exerts a ~4.23% change in pCO_2 (Takahashi et al., 1993), the efficacy at which seasonal temperature variation impacts pCO_2 is held constant at preindustrial levels by using the constant, climatological $\overline{\overline{pCO_{2\,AM\,PI}}}$ value in these calculations; rather than the transient $pCO_{2\,AM}$ value that increases over time (Figure 1a). This approach provides a hybrid estimate of the thermal pCO_2 component ($pCO_{2\,T\,Hybrid}$), which has a seasonal cycle amplitude that reflects preindustrial chemical leverage while still allowing transient changes in monthly sea surface temperature (SST) to alter the amplitude, structure, and phase of the seasonal cycle. $\overline{\overline{pCO_{2\,AM\,PI}}}$ is subtracted from the resulting $pCO_{2\,T\,Hybrid}$ values to isolate the thermal component monthly anomalies relative to $\overline{\overline{pCO_{2\,AM\,PI}}}$. This is done for each model grid and year of the simulation yielding a time series of the thermal pCO_2 component monthly anomalies in the absence of anthropogenic chemical leverage ($\Delta pCO_{2\,T\,\emptyset\,Anom.}$).

$$\Delta pCO_{2\,T\,\emptyset\,Anom.} = pCO_{2\,T\,Hybrid} - \overline{\overline{pCO_{2\,AM\,PI}}} \quad (1)$$

The $\Delta pCO_{2\,T\,\emptyset\,Anom.}$ values are then added to $pCO_{2\,AM}$ to get an evolving time series of the thermal pCO_2 component with seasonal cycle anomalies that reflect preindustrial chemical leverage and transient changes in SST ($pCO_{2\,T\,\emptyset}$; Figures 2b–2d).

$$pCO_{2\,T\,\emptyset} = \Delta pCO_{2\,T\,\emptyset\,Anom.} + pCO_{2\,AM} \quad (2)$$

To quantify the magnitude of BP component chemical leverage, we allow changes in ocean physics and biology to influence the transient pCO_2 seasonal cycle amplitude, structure, and phase while holding the sensitivity of pCO_2 to DIC and TA changes at preindustrial levels. The sensitivity of pCO_2 to changes in DIC (Egleston et al., 2010; Fassbender et al., 2017) and TA (Egleston et al., 2010; Hagens & Middelburg, 2016; Middelburg et al., 2020; Omta et al., 2010; Orr, 2011) increases as C_{ant} accumulates in the ocean such that the same relative change in DIC or TA exerts a larger magnitude relative change in pCO_2 over time. These sensitivities are held constant by applying preindustrial monthly climatologies of the Revelle Factor (RF; Bolin & Eriksson, 1958; Broecker et al., 1979; Frankignoulle, 1994; Sundquist et al., 1979) and Alkalinity Factor (AF; Takahashi et al., 1993) with

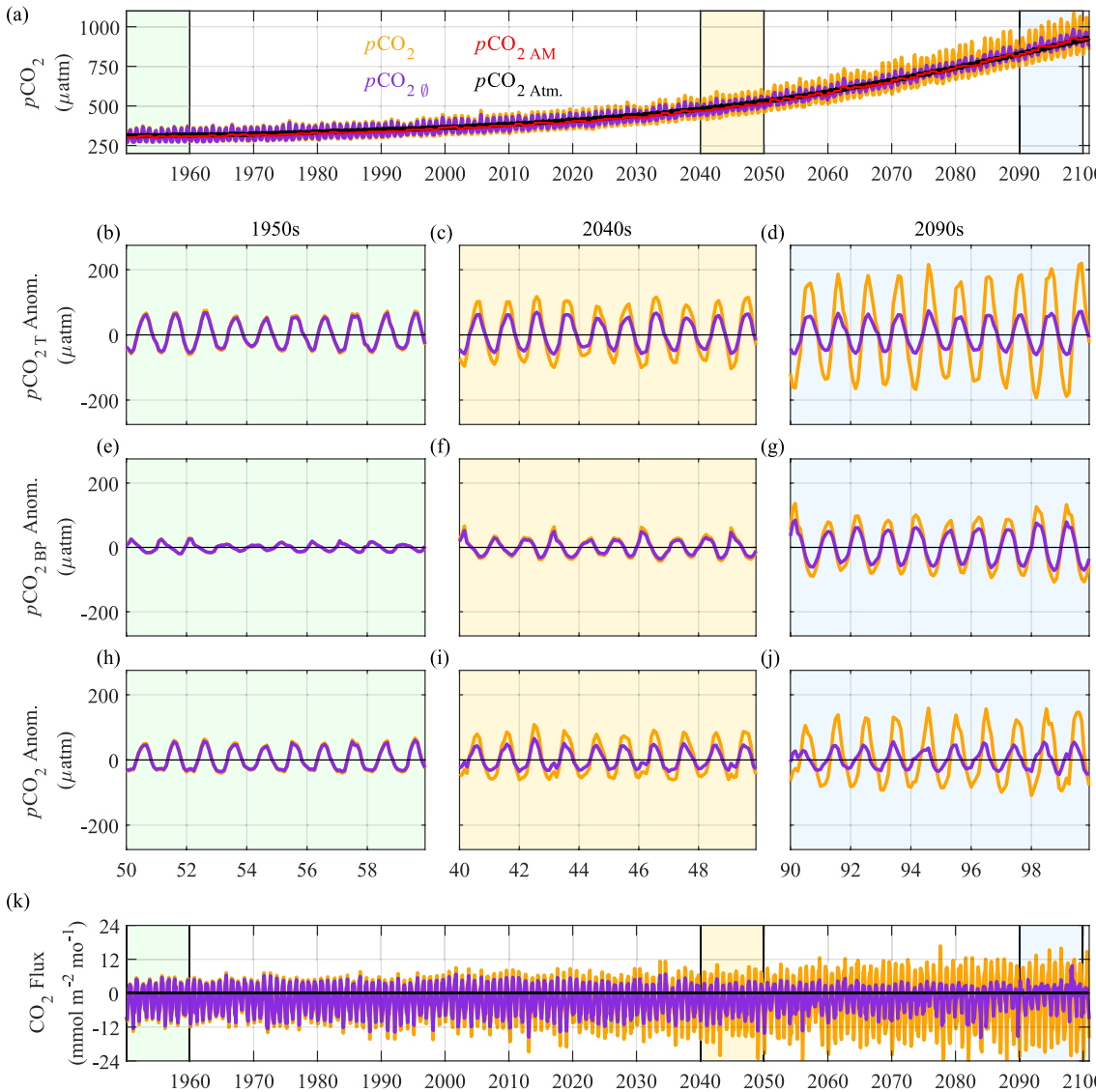

Figure 2. Time series of (a) transient (orange), no-leverage (Ø; purple), annual mean (AM; red), and atmospheric (Atm.; black) carbon dioxide partial pressure (pCO_2) from a grid in the central, subtropical North Pacific (170.5°W, 29.5°N). Time series of (b–d) thermal pCO_2 component (T) (e–g) biophysical pCO_2 component (BP), and (h–j) total pCO_2 seasonal anomalies (Anom.) relative to $pCO_{2\,AM}$ for the transient (orange) and no-leverage (purple) conditions during the decades highlighted in (a). (k) CO_2 flux for the transient and no-leverage conditions. Ensemble member 1 result shown.

the transient sensitivity of pCO_2 to salinity (Salinity Factor: SF; Takahashi et al., 1993). These sensitivity factors all take the same form (where overbars denote annually averaged values), with an example for the AF given here:

$$\mathrm{AF} = \left(\frac{\Delta pCO_2}{\overline{pCO_2}}\right) \times \left(\frac{\Delta \mathrm{TA}}{\overline{\mathrm{TA}}}\right)^{-1} \quad (3)$$

Monthly anomalies (Δ) in DIC, TA and SSS (relative to their annual mean values) are multiplied by their corresponding sensitivity factors as well as $pCO_{2\,AM}$ to calculate the corresponding monthly pCO_2 anomalies. This is done for each model grid and year of the simulation yielding a time series of the biophysical pCO_2 component monthly anomalies (relative to $pCO_{2\,AM}$) in the absence of anthropogenic chemical leverage ($\Delta pCO_{2\,BP\,\emptyset\,Anom.}$).

$$\Delta pCO_{2\,BP\,\emptyset\,Anom.} = pCO_{2\,AM} \times \left(\left[\mathrm{RF_{PI}} \times \left(\frac{\Delta \mathrm{DIC}}{\overline{\mathrm{DIC}}}\right)\right] + \left[\mathrm{AF_{PI}} \times \left(\frac{\Delta \mathrm{TA}}{\overline{\mathrm{TA}}}\right)\right] + \left[\mathrm{SF} \times \left(\frac{\Delta \mathrm{SSS}}{\overline{\mathrm{SSS}}}\right)\right]\right) \quad (4)$$

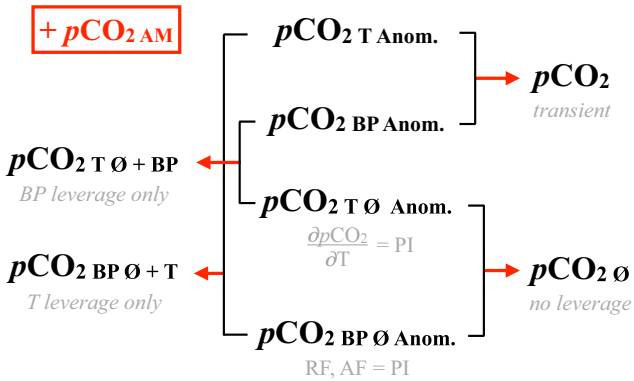

Figure 3. Thermal (T) and biophysical (BP) pCO_2 component monthly anomalies (relative to $pCO_{2\ AM}$) are calculated under transient conditions and with modifications that remove the influence of anthropogenic chemical leverage (Ø). $pCO_{2\ T\ Ø\ Anom.}$ holds the sensitivity of carbon dioxide partial pressure (pCO_2) to seasonal temperature variation ($\partial pCO_2/\partial T$) at its preindustrial (PI) value in each grid cell, while still allowing temperature to change over time. $pCO_{2\ BP\ Ø\ Anom.}$ holds the sensitivity of pCO_2 to seasonal dissolved inorganic carbon (DIC) and total alkalinity (TA) variations at its PI value in each grid cell, via the Revelle Factor (RF) and Alkalinity Factor (AF), while still allowing DIC and TA to change over time. Component anomalies are combined and $pCO_{2\ AM}$ is added to get the total pCO_2 time series with and without anthropogenic chemical leverage.

The $\Delta pCO_{2\ BP\ Ø\ Anom.}$ values are then added to $pCO_{2\ AM}$ to get an evolving time series of the biophysical pCO_2 component with seasonal cycle anomalies that reflect preindustrial chemical leverage and transient changes in ocean physics and biology ($pCO_{2\ BP\ Ø}$; Figures 2e–2g).

$$pCO_{2\,BP\,Ø} = \Delta pCO_{2\,BP\,Ø\,Anom.} + pCO_{2\,AM} \quad (5)$$

Chemical leverage for the thermal and biophysical pCO_2 terms can also be altered by natural variability, in addition to climate change and the direct influence of C_{ant}. For example, a change in the depth of seasonal entrainment could cause the $pCO_{2\ AM}$ value to rise or fall or alter the seasonal cycle of RF and AF. While we average across 30 ensemble members to reduce the influence of natural variability, if the ensemble mean contains the imprint of natural variability, our method does not differentiate such changes in chemical leverage from those induced by climate change. However, the end-of-century perturbations (relative to the PI period) to global mean $pCO_{2\ AM}$ (~600 µatm), RF (~5), and AF (~−5) are ≥10 times larger in magnitude than what would be expected from natural variability throughout most of the ocean (Figure S3 in Supporting Information S1).

3.4. Isolating Mechanisms

The evolution of total sea surface pCO_2 in the absence of anthropogenic chemical leverage ($pCO_{2\ Ø}$) is computed as the sum of $pCO_{2\ BP\ Ø\ Anom.}$, $pCO_{2\ T\ Ø\ Anom.}$, and $pCO_{2\ AM}$ (Figure 3). We also compute the transient biophysical ($pCO_{2\ BP\ Anom.}$) and thermal ($pCO_{2\ T\ Anom.}$) component anomalies by substituting time evolving values where preindustrial values were used for the no-leverage calculations (Equations 1 and 4; Figure 1e). $pCO_{2\ BP\ Anom.}$, $pCO_{2\ T\ Anom.}$, and $pCO_{2\ AM}$ are summed to yield the total transient sea surface pCO_2 time series (Figure 3). Differences between the reconstructed pCO_2 and $pCO_{2\ Ø}$ time series reflect the contribution of C_{ant}-induced chemical leverage to pCO_2 seasonal cycle changes (e.g., Figure 2a). We also sum different pairings of the transient and no-leverage anomaly terms to isolate the impacts of biophysical and thermal C_{ant}-induced chemical leverage individually (Figure 3).

The deconstruction and reconstruction of pCO_2, as required to isolate and attribute drivers of the seasonal carbon cycle feedback, causes minor inconsistencies (-2.1 ± 3.2 µatm, area-weighted global mean over all time) between the model output and the offline computations of pCO_2 (Figure S4 and S5 in Supporting Information S1), which in turn influence the sea-air CO_2 flux. We discuss bias correction of the reconstructed pCO_2 values and subsequent calculation of sea-air CO_2 fluxes in Text S2 of Supporting Information S1. We find excellent agreement ($r = 0.99$, $p < 0.01$) between the model output and our reconstructed transient sea-air CO_2 fluxes (Figure S6 in Supporting Information S1) with a 1% difference in cumulative ocean carbon uptake by the end of the century (Figure S7 in Supporting Information S1). All fluxes are multiplied by the local, time-evolving ice fraction prior to regional averaging or quantification of cumulative ocean carbon uptake. In the *Results and Discussion* section, $\pm 1\sigma_{xy}$ is used to signify global spatial variation in the ensemble mean result and $\pm 1\sigma_{ens}$ is used to signify ensemble member variation in globally integrated or averaged values.

4. Results

By the end of the 21st century, ESM2M ensemble mean changes in the transient pCO_2 seasonal cycle amplitude (A-pCO_2) range from −25 to 669 µatm with a spatially averaged global mean increase ($\pm 1\sigma_{xy}$) of 62 ± 49 µatm, relative to the 1950s (Figure 4a). This translates to amplitude changes ranging from −30% to well over 100% with a spatially averaged global mean increase ($\pm 1\sigma_{xy}$) of 115 ± 67% (Figure 4b). Regions of the equatorial Pacific and Southern Ocean are anomalous, exhibiting negligible amplitude increases and declines in some areas. Similarly ubiquitous A-pCO_2 amplification was found by Gallego et al. (2018) across an ensemble of seven CMIP5 models over a shorter time horizon (~2010s–2090s). Ensemble mean changes in thermal and biophysical pCO_2 component amplitudes are even larger than changes in the overall A-pCO_2, reaching over 300 µatm in some regions

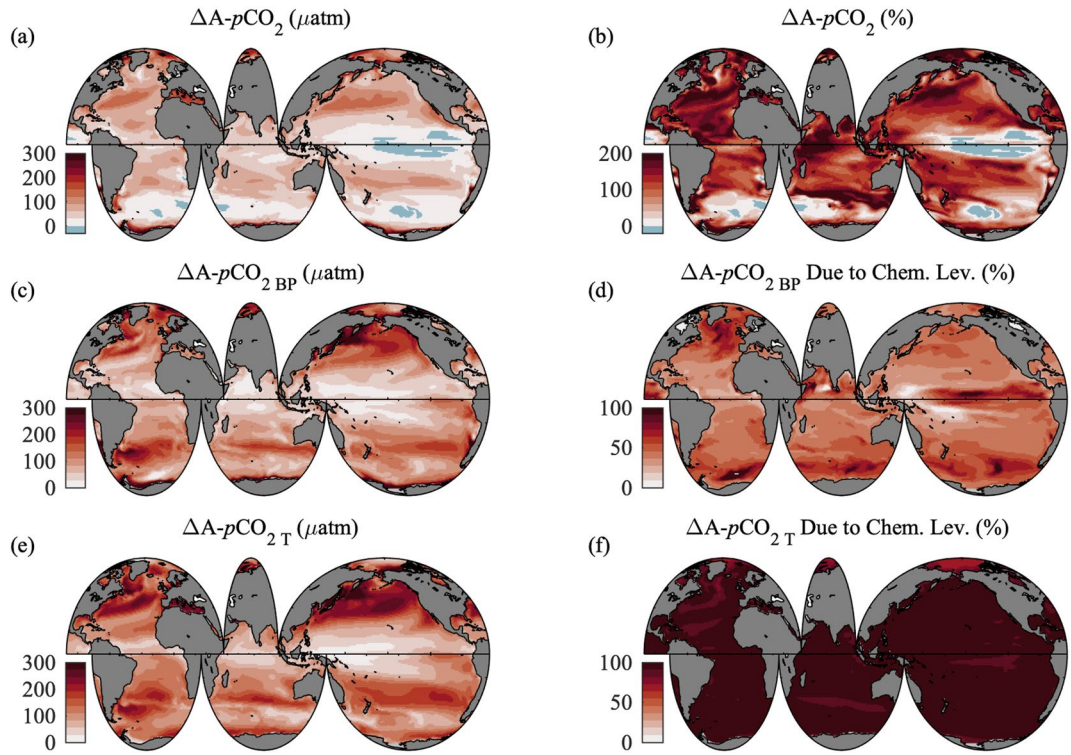

Figure 4. 1950s to 2090s change in the transient pCO_2 seasonal cycle amplitude (ΔA-pCO_2), in units of (a) µatm and (b) percent. 1950s to 2090s change in (c) ΔA-$pCO_{2\,BP}$ (µatm) and (e) ΔA-$pCO_{2\,T}$ (µatm). Percent of (d) ΔA-$pCO_{2\,BP}$ and (f) ΔA-$pCO_{2\,T}$ attributed to C_{ant}-induced chemical leverage (Chem. Lev.). These and all subsequent maps were made using the *cmocean* colormap package (Thyng et al., 2016). Ensemble mean result shown.

(Figures 4c and 4e). The much larger magnitude changes in A-$pCO_{2\,BP}$ (global spatial average: 102 µatm, 250%) and A-$pCO_{2\,T}$ (global spatial average: 122 µatm, 247%), relative to the 1950s, emphasize the counterbalance between drivers, which compete to yield the overall pCO_2 seasonal cycle amplitude, structure, and phase (e.g., Figure 2).

Anthropogenic chemical leverage is responsible for 45 ± 88% of the biophysical and 100 ± 11% of the thermal pCO_2 component seasonal cycle amplification when taking the global spatial average ($\pm 1\sigma_{xy}$) of the ensemble mean result (Figures 4d and 4f). These percentage values are derived by differencing the transient and no-leverage A-pCO_2 changes (1950s to 2090s) and dividing by the transient A-pCO_2 change for each of the thermal and biophysical components. Although we are comparing amplitude changes at specific locations in a dynamic medium where gyre or biome boundaries may change over time, the meridional gradients in RF, AF, and $pCO_{2\,AM}$ are relatively smooth (Figures S3a–S3c in Supporting Information S1), such that gyre boundary changes are unlikely to dominate the large-scale patterns identified in Figure 4. Our results suggest that changes in the seasonal SST cycle (Figure S8i in Supporting Information S1) contribute negligibly to thermal component amplification. Instead, rising $pCO_{2\,AM}$ values (and the resulting enhanced sensitivity to temperature) explain nearly all the thermal pCO_2 component amplification (Figure 4f). In contrast, reductions in the ocean buffer capacity (increases in RF and decreases in AF) can explain only half of the biophysical pCO_2 component amplification, revealing that modeled changes in ocean physics and biology caused by climate change contribute significantly to the modification of pCO_2 seasonal cycles.

Cumulative sea-air CO_2 fluxes computed from the transient and no-leverage pCO_2 time series reveal that pCO_2 seasonal cycle modifications caused by C_{ant} accumulation increase the ocean carbon sink strength by 8.1 ± 0.4% (37 ± 2 PgC; $\pm 1\sigma_{ens}$). The ESM2M cumulative global ocean carbon sink from 1950 to 2100 is 493 ± 1 PgC ($\pm 1\sigma_{ens}$) with anthropogenic chemical leverage and 456 ± 1 PgC ($\pm 1\sigma_{ens}$; Figures 5a and 5b) with preindustrial chemical leverage. Thus, C_{ant}-induced changes to the pCO_2 seasonal cycle increase carbon uptake throughout much of the ocean relative to an ocean with preindustrial chemical leverage experiencing the same physical and

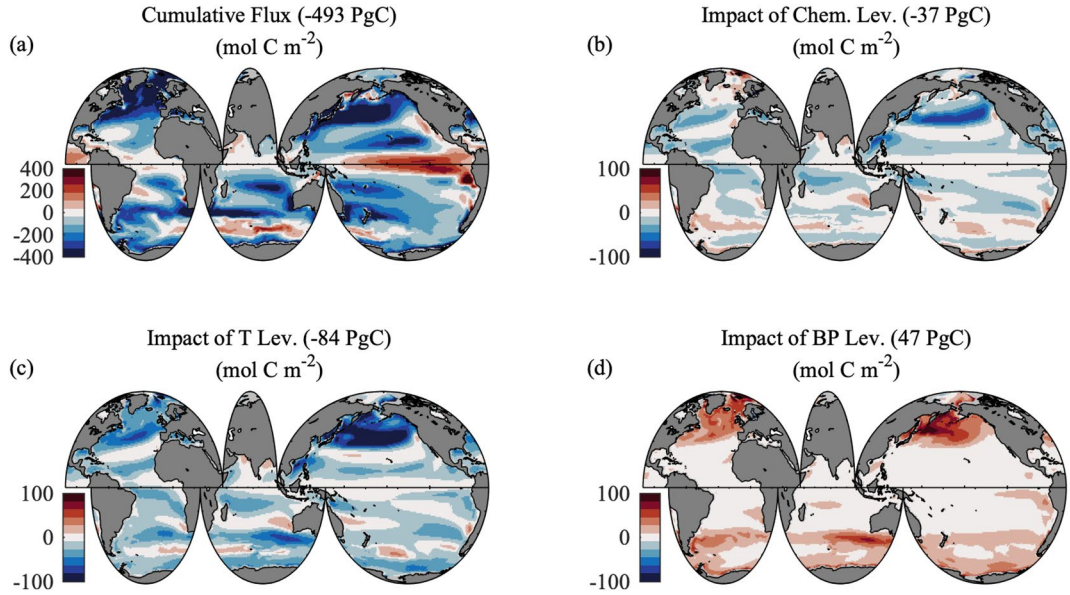

Figure 5. (a) Transient cumulative (1950 to 2100) flux and the (b) difference between the transient cumulative flux and the cumulative flux with no anthropogenic chemical leverage. Impact of adding (c) thermal component and (d) biophysical component chemical leverage to the no-leverage configuration. For b through d, red colors indicate a weaker sink (or stronger source) and blue colors indicate a stronger sink (or weaker source) relative to the no-leverage configuration. Ensemble mean result shown with globally integrated values given in PgC. Standard deviation across ensemble members shown in Figure S9 of Supporting Information S1.

biological changes over this period. However, the flux discrepancy is not evenly distributed; the mid-latitude North Pacific carbon sink increase caused by chemical leverage is ~15% (Figure 5b). This result is intriguing because the RF increases fastest in the high-latitudes (Bittig et al., 2018; Fassbender et al., 2017), which causes less efficient mean-state C_{ant} uptake over time (Figure S3 in Supporting Information S1). Our result suggests that seasonal alteration of the marine carbon cycle, in the North Pacific and globally, works in opposition to the larger mean-state Revelle feedback that is expected to reduce 21st century ocean carbon uptake significantly (by up to ~60%; Figure 2c in Rodgers et al., 2020).

To diagnose what is causing this result, we evaluate driver-specific influences on sea-air CO_2 flux using different combinations of pCO_2 component monthly anomalies (Figure 3). We calculate the sea-air flux using the thermal leverage ($pCO_{2\,T+BP\,\emptyset}$) and biophysical leverage ($pCO_{2\,T\,\emptyset+BP}$) pCO_2 time series (Figures 5c and 5d). The thermal driver works to make pCO_2 values lowest during winter through enhanced solubility and highest during summer through reduced solubility. The biophysical drivers generally work to make pCO_2 values highest during winter due to deep mixing and lowest during spring and summer due to biological productivity. Therefore, allowing only thermal or biophysical pCO_2 component amplification to occur will magnify the seasonality associated with that driver. Since wind speeds are highest during winter, which increases the impact of wintertime disequilibrium on the annual net sea-air CO_2 flux, it is expected that thermal amplification alone would cause a net increase in ocean carbon uptake and biophysical amplification alone would cause a net decrease in ocean carbon uptake.

Relative to the no-leverage conditions, the cumulative ocean carbon sink is 18% stronger (84 ± 2 PgC increase in uptake; $\pm 1\sigma_{ens}$) with thermal pCO_2 component chemical leverage and 10% weaker (47 ± 2 PgC decrease in uptake; $\pm 1\sigma_{ens}$) with biophysical pCO_2 component chemical leverage by the year 2100. The largest impacts for these combinations are found in the high latitudes (particularly the North Pacific Ocean) where the sensitivity of pCO_2 to DIC and SST is highest (Gallego et al., 2018) and DIC and SST seasonal cycles are large (Figure S8 in Supporting Information S1), allowing chemical leverage to be expressed strongly. The imbalance between cumulative flux impacts resulting from thermal versus biophysical C_{ant}-induced chemical leverage, particularly in the North Pacific (Figures 5c and 5d), leads to greater carbon uptake under transient (vs. no-leverage) conditions (Figure 5b). This imbalance is caused by ~50% of biophysical pCO_2 component amplification being driven by processes other than C_{ant} increases, such as modulation of the ocean physics and biology (Figure 4d).

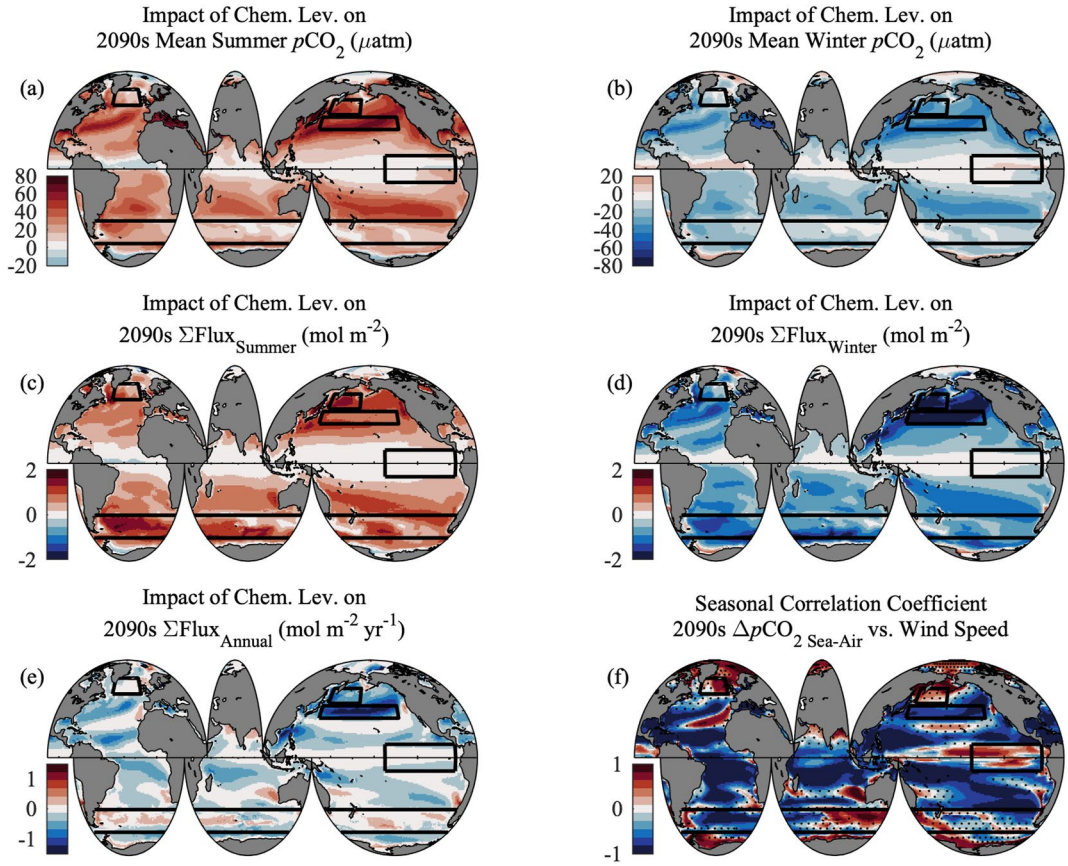

Figure 6. 2090s difference between the transient and no-leverage: (a) warm and (b) cool season carbon dioxide partial pressure (pCO_2) values; cumulative (c) warm and (d) cool season CO_2 fluxes; and (e) cumulative annual CO_2 flux. The northern hemisphere warm season is defined as the months May to October and the cool season is defined as the months November to April (within a given calendar year). These periods are swapped for the southern hemisphere. Negative 2090s cumulative annual CO_2 flux values indicate that the transient sink is larger than the no-leverage sink. (f) 2090s local seasonal $\Delta pCO_{2\ Sea\text{-}Air}$ versus wind speed correlation coefficients. Positive correlations indicate high wind speeds during periods with high surface ocean pCO_2 values. Regions with insignificant correlations (p-values > 0.05) are stippled. Boxes emphasize regions of interest discussed in the text. Ensemble mean result shown.

To understand mechanistically how modifications to the seasonality of pCO_2 impact the ocean carbon sink regionally, we consider pCO_2 seasonal cycle changes in relation to seasonal wind speed variation. We focus on seasonal differences between the transient and no-leverage conditions where the northern hemisphere warm period is defined as the months May to October and the cold period is defined as the months November to April (within a given calendar year). These periods are swapped for the southern hemisphere. We highlight results from the subtropical and subpolar North Pacific, where the largest carbon sink response is found (Figure 4b), as well as key carbon cycle regions, including the subpolar North Atlantic, Southern Ocean, and Equatorial Pacific.

By the 2090s, pCO_2 values are higher during summer and lower during winter due to C_{ant}-induced seasonal cycle changes throughout most of the global surface ocean (Figures 6a and 6b); minimal differences are found in the tropics. This aligns with expectations since C_{ant}-induced thermal amplification outcompetes C_{ant}-induced biophysical amplification in most regions and thermal amplification works to increased summer highs and decrease winter lows. What is somewhat unintuitive; however, is how the ocean carbon sink is enhanced when changes in seasonal pCO_2 highs are of greater magnitude than changes in seasonal pCO_2 lows. The answer to this question requires a closer look at regional relationships between seasonal pCO_2 and wind speed variation, as wind speeds are generally greatest during winter.

To make sense of the mechanisms driving the seasonal carbon cycle feedback, we first consider a simple theoretical example. In the thermally dominated subtropics, the previously identified C_{ant}-induced pCO_2 seasonal

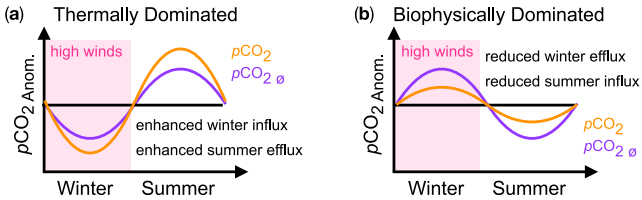

Figure 7. Theoretical example of surface ocean pCO_2 seasonal cycle anomalies (Anom.; realtive to $pCO_{2\,AM}$) in (a) thermally and (b) biophysically dominated regions of the ocean. Based on results from Figures 6a and 6b, chemical leverage results in higher summer pCO_2 values and lower winter pCO_2 values relative to the no-leverage condition ($pCO_{2\,ø}$). For both cases, the wintertime sink strength and the summertime source strength are enhanced by chemical leverage. Pink shading emphasizes that higher wind speeds often occur during winter.

cycle changes (Figures 6a and 6b) will result in higher summer highs and lower winter lows; an expansion of the seasonal cycle relative to the no-leverage conditions (Figure 7a). Here, high winter wind speeds generally correspond to minimum pCO_2 values, giving greater efficacy to the CO_2 sink season. In the biophysically dominated high latitudes, which have the opposite seasonal pCO_2 phasing (Takahashi et al., 2002), C_{ant}-induced pCO_2 seasonal cycle changes will result in higher summer lows and lower winter highs; a compression of the seasonal cycle relative to the no-leverage conditions (Figure 7b). Here, high winter wind speeds generally correspond to maximum pCO_2 values, giving greater efficacy to the CO_2 source season. In both cases, seasonal cycle changes (relative to the no-leverage conditions) work to increase the ocean carbon sink during the season with maximum wind speeds. Regional relationships between seasonal wind speed and pCO_2 phasing should therefore play a fundamental role in how C_{ant}-induced pCO_2 seasonal cycle changes impact the global ocean carbon sink.

With this theoretical understanding, we can now evaluate the results from specific regions of the ocean. In the thermally dominated subtropics, there is an expansion of $\Delta pCO_{2\,\text{Sea-Air}}$ seasonal cycle amplitudes (higher highs and lower lows) relative to the no-leverage conditions and increases in the maximum values greatly exceed decreases in the minimum values (Figures 8g and 8h, Figures S11, and S12 in Supporting Information S1). In the biophysically dominated subpolar North Pacific Ocean, there is a contraction of $\Delta pCO_{2\,\text{Sea-Air}}$ seasonal cycle amplitude (lower highs and higher lows; Figures 8d and 8e) relative to the no-leverage conditions. The seasonal cycle is similarly altered in the biophysically dominated Southern Ocean and subpolar North Atlantic Ocean (lower highs and higher lows; Figure 8); however, in the Southern Ocean, where pCO_2 seasonal cycles are weak to begin with, these changes are enough to reverse the pCO_2 seasonal cycle phasing. Here, seasonal correlations between $\Delta pCO_{2\,\text{Sea-Air}}$ and wind speed and are not always statistically significant due to complex pCO_2 seasonal cycles, leading to a heterogenous flux response (Figure 6e). In the Equatorial Pacific, the pCO_2 seasonal cycle is small and wind speeds are almost constant throughout the year, causing relatively minor differences between the transient and no-leverage pCO_2 values and fluxes (Figures 8j and 8k). These results align with theoretical expectations for most regions, causing a net increase in 2090s annual carbon uptake relative to the no-leverage conditions (Figure 6e). Our results indicate that changes in wintertime carbon fluxes outcompete changes in summertime carbon fluxes, yielding an overall greater ocean carbon sink due to anthropogenic chemical leverage.

5. Discussion

Differences between the transient and no-leverage pCO_2 values and sea-air CO_2 fluxes in our analysis are caused exclusively by the implementation of transient versus preindustrial sensitivity terms (Figure 1e, Equations 1 and 4). The ~50% increase in RF and AF magnitudes between the PI and 2090s (Figure 8) allows the same seasonal DIC and TA variations (Figures S8a–S8f in Supporting Information S1) to have different impacts on pCO_2 in the transient and no-leverage calculations during each year of the simulation. Similarly, over a tripling in the $pCO_{2\,AM}$ sensitivity to temperature from the PI to the 2090s (Figure 8) causes a much larger pCO_2 solubility response to seasonal temperature swings (Takahashi et al., 1993), which overwhelms the impact of small changes in A-SST (Figure S8i in Supporting Information S1) on the overall change in A-pCO_2. While there are notable changes in A-SST, A-DIC, A-TA, and the maximum depth of seasonal mixing by the 2090s (Figures S8i, S8a–S8f, S8p–S8r in Supporting Information S1), these changes are incorporated into both the transient and no-leverage calculations (Equations 1 and 4) and, thus, do not contribute to differences between pCO_2 and $pCO_{2\,ø}$.

The total pCO_2 seasonal cycle amplification (caused by C_{ant} accumulation and climate change) for the thermal term is larger than that of the biophysical term in nearly all ocean regions (Figures 4c and 4e). Additionally, C_{ant} is responsible for 100% of the thermal component amplification and only ~50% of the biophysical component amplification. Combined, these factors cause C_{ant}-induced chemical leverage to be larger for the thermal pCO_2 component than the biophysical pCO_2 component (Figure 8 left column); the imbalance being largest in the North Pacific (Figure 5c and 5d) where A-SST is largest (Figures S8g and S8h in Supporting Information S1). With the highest seasonal wind speeds generally occurring during winter when the thermal pCO_2 component is low due to

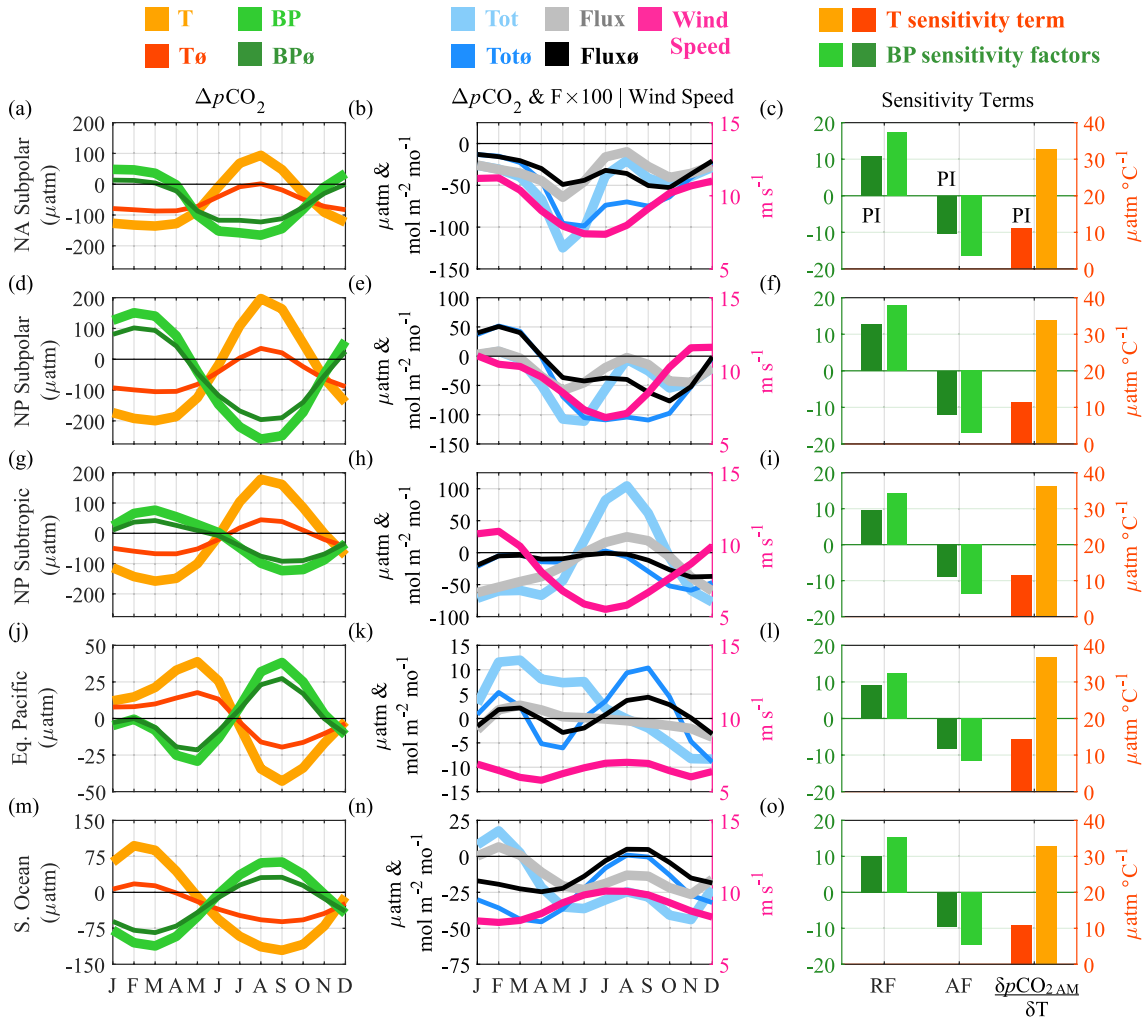

Figure 8. Regional 2090s $\Delta pCO_{2\ \text{Sea-Air}}$ seasonal cycles for the (left) thermal (T), biophysical (BP), and (middle) total (Tot) carbon dioxide partial pressure (pCO_2) terms as well as the sea-air CO_2 flux seasonal cycle (times 100; $F \times 100$), all with and without (Ø) anthropogenic chemical leverage. Note different y-axis ranges for subplots in left and middle columns. Regional 2090s seasonal cycles for wind speed (right axis) are also shown in the middle subplots. (right) Regional sensitivity terms for the 2090s and preindustrial period (PI) including the annual mean Revelle Factor (RF) and Alkalinity Factor (AF) and the sensitivity of $pCO_{2\ \text{AM}}$ to temperature (right axis). Regions correspond to the boxes in Figure 6. Ensemble mean result shown.

enhanced solubility (Figure 6f), the net impact of C_{ant}-induced pCO_2 seasonal cycle changes is an increase in the global ocean carbon sink strength caused primarily by wintertime sink enhancement. This result aligns with the findings of similarly focused modeling studies by Rodgers et al. (2008) and Gorgues et al. (2010).

One factor to consider when comparing seasonal carbon cycle feedback magnitudes quantified from different models or simulation experiments is the role of wind speed (structure and magnitude). Wind speed is a scalar in flux computations (Text S2 in Supporting Information S1) and its pattern and evolution (e.g., Figures S8j–S8l in Supporting Information S1) will influence how ocean pCO_2 and $pCO_{2\ Ø}$ differences contribute to the overall feedback magnitude ($\Sigma\text{Flux} - \Sigma\text{Flux}_Ø$) for each simulation evaluated. Thus, when comparing results across models or simulation experiments, expressing the feedback as a percentage of the transient cumulative carbon uptake ($100 \times (\Sigma\text{Flux} - \Sigma\text{Flux}_Ø)/\Sigma\text{Flux}$) will normalize for dissimilar wind speed representation impacts. As a test of our methodology, we evaluate one simulation of ESM2M under historical-RCP4.5 forcing. We find similar results and driving mechanisms to those from the historical-RCP8.5 scenario, with a cumulative ocean carbon sink enhancement of 5% (20 PgC) by 2100 due to the seasonal carbon cycle feedback (Figure S10 in Supporting Information S1). This suggests that the seasonal carbon cycle feedback remains discernible in more modest CO_2 forcing experiments and the mechanisms driving the feedback are consistent with the RCP8.5 scenario.

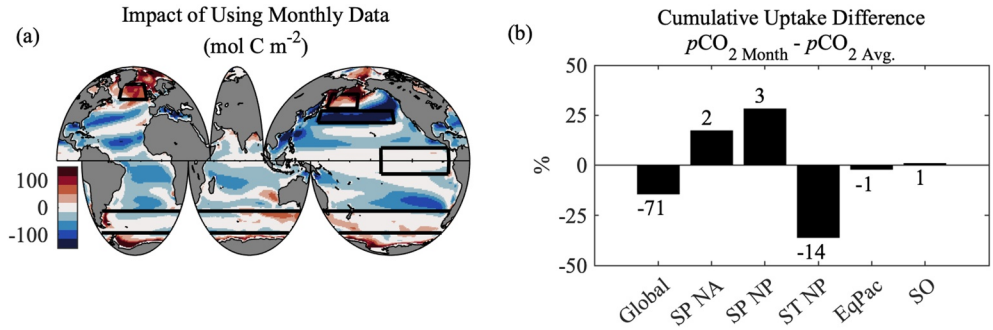

Figure 9. (a) Cumulative 1950 to 2100 ocean carbon uptake discrepancy between fluxes calculated using monthly resolved versus annual mean sea surface pCO_2 values. Negative values indicate more carbon uptake when using monthly resolved pCO_2 values, meaning that annual mean pCO_2 values would underestimate the carbon sink strength. (b) Cumulative uptake difference in percent for the boxed regions on the map (SP: subpolar; ST: subtropic; NA: North Atlantic; NP: North Pacific; EqPac: Equatorial Pacific; SO: Southern Ocean). Numbers above and below the bars are carbon uptake differences in units PgC. Ensemble mean result shown.

Our results indicate that large (>100% on average) changes in A-pCO_2 cause a modest (<10%) increase in cumulative ocean carbon uptake from 1950 to 2100. This is because seasonal wind speed variation systematically enhances the impact of C_{ant}-altered pCO_2 seasonal cycles during wintertime, which helps to combat larger magnitude summertime increases in pCO_2. Thus, regional relationships between wind speed and $\Delta pCO_{2\ \text{Sea-Air}}$ seasonality (Figure 6f) play a key role in compensating the seasonal fluxes (Figures 6c and 6d) that result from largely asymmetric changes in pCO_2 extrema (Fassbender et al., 2018; Figure S11 in Supporting Information S1), particularly in the subtropics. Considering this significant seasonal flux compensation, we test whether the same result can be reproduced by using annual mean pCO_2 values instead of monthly pCO_2 values. Recalculating the cumulative ocean carbon uptake through 2100 using transient monthly gas transfer velocities (Text S2 in Supporting Information S1) with annually averaged pCO_2 values ($pCO_{2\ \text{Avg.}}$, not to be confused with $pCO_{2\ \text{AM}}$ values) causes a 15.9 ± 0.4% ($\pm 1\sigma_{ens}$) underestimation of the carbon sink relative to the case when using monthly resolved pCO_2 values (Figure 9). As seasonal pCO_2 extrema diverge, annual mean values become exceedingly less representative of ocean conditions and seasonally varying winds cannot fully compensate for the use of $pCO_{2\ \text{Avg.}}$ values (Figure S7 in Supporting Information S1). While the global cumulative flux bias is relatively small (~15%), it is nontrivial regionally (Figure 9b; Fassbender et al., 2018), with values near or exceeding ±20% in the subtropical North Pacific and subpolar North Pacific and North Atlantic. The divergence between cumulative fluxes computed from $pCO_{2\ \text{Avg.}}$ versus monthly resolved pCO_2 values provides another perspective (relative to prior figures) on how the pCO_2 seasonal cycle effects the strength of the ocean carbon sink.

6. Conclusions

Results from our ESM2M case study demonstrate that the impacts of transient thermal and biophysical pCO_2 component seasonal cycle amplification primarily work in opposition to each other and are greatest in the high latitudes where the sensitivity of pCO_2 to DIC and SST is highest (Gallego et al., 2018) and DIC and SST seasonal cycles are large, allowing chemical leverage to be expressed more strongly (Figure S8 in Supporting Information S1). Biophysical component chemical leverage decreases the ocean carbon sink strength while thermal component chemical leverage increases the ocean carbon sink strength. Combined, these processes result in a cumulative global ocean carbon sink that is 8.1 ± 0.4% ($\pm 1\sigma_{ens}$) greater than a hypothetical ocean with preindustrial chemical leverage. Using the ensemble allows us to characterize the robustness of our method to changes driven by internal climate variability and its potential applicability to individual model simulations. Each of the 30 ESM2M ensemble members identified the same broad scale pattern of cumulative carbon uptake with very small across simulation differences (Figure S9 in Supporting Information S1). Variability ($\pm 1\sigma_{ens}$) in the ensemble mean global cumulative carbon uptake response (−37 ± 2 PgC) was confined to ±5%, suggesting that this method could be reliably applied to individual Earth System Model simulations.

In the ESM2M historical-RCP8.5 experiment, the 1950s to 2090s global mean change in sea surface pCO_2 seasonal cycle amplitude is 115 ± 67% (spatial average $\pm 1\sigma_{xy}$ of the ensemble mean result), which includes

regions of the Southern Ocean and equatorial Pacific where contraction of the seasonal cycle is projected. Additionally, changes in the pCO_2 seasonal maxima are larger in magnitude than changes in the seasonal minima, relative to hypothetical conditions in which the ocean experiences no chemical leverage from rising C_{ant} (Figure S11 and S12 in Supporting Information S1). However, the influence of C_{ant}-induced pCO_2 seasonal cycle changes on the cumulative ocean carbon sink by the year 2100 is a small increase ($8.1 \pm 0.4\%$; $\pm 1\sigma_{ens}$) due to the compensating effect of wind speed seasonality on sea-air fluxes. Impacts in some regions were larger, with the North Pacific exhibiting a ~15% increase in sink strength due to a greater imbalance in C_{ant}-induced $pCO_{2\,T}$ and $pCO_{2\,BP}$ term amplification. Importantly, the flux compensation caused by wind speed seasonality does not indicate that annually averaged pCO_2 values can be used in flux calculations; this will lead to increasingly inaccurate estimates of the ocean carbon sink strength (Figure S7 in Supporting Information S1). The global bias resulting from the use of annual versus monthly-resolved pCO_2 values is a $15.9 \pm 0.4\%$ ($\pm 1\sigma_{ens}$) underestimate of the 2100 ESM2M cumulative ocean carbon sink, while regional biases can exceed ~20% in either direction (Figure 9).

Our methodology makes it possible to quantify the fraction of pCO_2 seasonal cycle changes caused by increased sensitivity of the marine carbonate system to thermal and biophysical drivers because of C_{ant} accumulation, and to further deconstruct these seasonal perturbations into components arriving from changes in: (a) temperature itself, (b) the sensitivity of pCO_2 to changes in temperature, (c) the sensitivity of pCO_2 to biophysical drivers, and (d) ocean physics and biology. We find that factors 2–4 account for the projected pCO_2 seasonal cycle changes. The thermal component amplification is driven almost entirely ($100 \pm 11\%$; $1\sigma_{xy}$) by rising ocean carbon content, and the enhanced temperature sensitivity this conveys, while only half ($45 \pm 88\%$; $1\sigma_{xy}$) of the biophysical amplification can be attributed to increasing sensitivity of the carbonate system to biophysical drivers. This indicates that projected changes in physical and biological ocean process play an important, direct role in how the nonthermal term evolves. Factors 2–4 (thermal sensitivity, biophysical sensitivity, and biophysical forcing) impact the evolving strength of the ocean carbon sink, however with significant modification by seasonally varying wind speed.

In summary, our approach isolates the influence of C_{ant} on seasonal drivers of pCO_2 variability in ESM2M to determine whether there is a net change in the annual sea-air CO_2 flux, which would reflect a seasonal contribution to the overall marine carbon cycle feedback. Recent estimates suggest that the full impact of C_{ant} accumulation on the decline in ocean buffer capacity (i.e., not just its impact on seasonal cycle extremes) can significantly reduce the ocean carbon sink efficiency (by up to ~60% from 1950 to 2100; Rodgers et al., 2020). However, on seasonal timescales, we find that C_{ant} accumulation works to modestly increase cumulative global ocean carbon uptake (by ~8%) in ESM2M, reflecting a negative (i.e., climate-change diminishing) seasonal marine carbon cycle feedback. Thus, in this model, the seasonal component of the full carbon cycle response to C_{ant} accumulation alleviates what would be a stronger, positive (i.e., climate-change enhancing) Revelle Factor feedback in the absence of carbonate system seasonality.

Different model representations of the modern CO_2 flux in high-latitude regions have been directly linked to projected differences (>150 PgC for CMIP5 models) in 21st century cumulative ocean carbon uptake under RCP8.5 forcing (Kessler & Tjiputra, 2016; Nevison et al., 2016). Application of our offline approach to other Earth System Models under RCP8.5 forcing will provide insight about whether the ESM2M result is representative, or if models exhibit a range of seasonal CO_2 flux feedback magnitudes that could meaningfully contribute to the across model spread in 21st century cumulative carbon uptake. While, ESM2M exhibits average performance in reproducing the observed surface ocean pCO_2 seasonal cycle (Pilcher et al., 2015) and the modern (1981–2014) global warming trend (Tokarska et al., 2020), modern fidelity to observed conditions is not necessarily an indication of future model performance. The seasonal CO_2 flux feedback should therefore be evaluated for a suite of Earth System Models and CO_2 concentration scenarios (as recently recommended by Jones & Friedlingstein, 2020) to constrain its magnitude and sign.

Data Availability Statement

All model data can be accessed at poseidon.princeton.edu. The MATLAB scripts used to process, analyze, and visualize model data for this work can be accessed at Zenodo (Fassbender, 2022) https://doi.org/10.5281/zenodo.6512476. Updates will be maintained at the GitHub repository https://github.com/ajfassbender/seasonal-co2-flux-feedback.

Acknowledgments
We thank two anonymous reviewers and the editor for insightful feedback that helped us improve manuscript clarity. We also thank Mar C. Arroyo and Jonathan D. Sharp for valuable feedback during the manuscript revision stage. A.J.F. was supported by the David and Lucile Packard Foundation and NOAA's Global Ocean Monitoring and Observing Program. S.S. was supported by NASA award NNX17AI75G and the Southern Ocean Carbon and Climate Observations and Modeling (SOCCOM) Project under the NSF Award PLR-1425989, with additional support from NOAA and NASA. Logistical support for the SOCCOM Project in the Antarctic was provided by the NSF through the U.S. Antarctic Program. K.B.R. was supported through IBS-R028-D1. This is PMEL Contribution 5204.

References

Archer, D. E. (2005). Fate of fossil fuel CO_2 in geologic time. *Journal of Geophysical Research*, *110*(C9), C09S05. https://doi.org/10.1029/2004JC002625

Archer, D. E., Eby, M., Brovkin, V., Ridgwell, A., Cao, L., Mikolajewicz, U., et al. (2009). Atmospheric lifetime of fossil fuel carbon dioxide. *Annual Review of Earth and Planetary Sciences*, *37*(1), 117–134. https://doi.org/10.1146/annurev.earth.031208.100206

Archer, D. E., Kheshgi, H., & Maier-Reimer, E. (1997). Multiple timescales for neutralization of fossil fuel CO_2. *Geophysical Research Letters*, *24*(4), 405–408. https://doi.org/10.1029/97gl00168

Arora, V. K., Boer, G. J., Friedlingstein, P., Eby, M., Jones, C. D., Christian, J. R., et al. (2013). Carbon-concentration and carbon-climate feedbacks in CMIP5 Earth system models. *Journal of Climate*, *26*(15), 5289–5314. https://doi.org/10.1175/JCLI-D-12-00494.1

Bittig, H. C., Steinhoff, T., Claustre, H., Fiedler, B., Williams, N. L., Sauzède, R., et al. (2018). An alternative to static climatologies: Robust estimation of open ocean CO_2 Variables and nutrient concentrations from T, S, and O_2 data using Bayesian neural networks. *Frontiers in Marine Science*, *5*, 1–29. https://doi.org/10.3389/fmars.2018.00328

Bolin, B., & Eriksson, E. (1958). Changes in the carbon dioxide content of the atmosphere and sea due to fossil fule combustion. In B. Bolin (Ed.), *The atmosphere and the sea in motion: Scientific contributions to the Rossby memorial volume* (pp. 130–142). Rockefeller Institute Press.

Broecker, W. S., Takahashi, T., Simpson, H. J. J., & Peng, T.-H.-H. (1979). Fate of fossil fuel carbon dioxide and the global carbon budget. *Science*, *206*(4417), 409–418. https://doi.org/10.1126/science.206.4417.409

Dickson, A. G., Wesolowski, D. J., Palmer, D. A., & Mesmer, R. E. (1990). Dissociation constant of bisulfate ion in aqueous sodium chloride solutions to 250°C. *Journal of Physical Chemistry*, *94*(20), 7978–7985. https://doi.org/10.1021/j100383a042

Dickson, A. G. G., & Millero, F. J. J. (1987). A comparison of the equilibrium constants for the dissociation of carbonic acid in seawater media. *Deep-Sea Research Part A. Oceanographic Research Papers*, *34*(10), 1733–1743. https://doi.org/10.1016/0198-0149(87)90021-5

Egleston, E. S., Sabine, C. L., & Morel, F. M. M. (2010). Revelle revisited: Buffer factors that quantify the response of ocean chemistry to changes in DIC and alkalinity. *Global Biogeochemical Cycles*, *24*(1), 1–9. https://doi.org/10.1029/2008GB003407

Fassbender, A. (2022). Seasonal CO2 Flux Feedback Code (v1.0). *Zenodo*. https://doi.org/10.5281/zenodo.6512476

Fassbender, A. J., Rodgers, K. B., Palevsky, H. I., & Sabine, C. L. (2018). Seasonal asymmetry in the evolution of surface ocean pCO_2 and pH thermodynamic drivers and the influence on sea-air CO_2 flux. *Global Biogeochemical Cycles*, *32*(10), 1476–1497. https://doi.org/10.1029/2017GB005855

Fassbender, A. J., Sabine, C. L., & Palevsky, H. I. (2017). Nonuniform ocean acidification and attenuation of the ocean carbon sink. *Geophysical Research Letters*, *44*(16), 8404–8413. https://doi.org/10.1002/2017GL074389

Frankignoulle, M. (1994). A complete set of buffer factors for acid/base CO_2 system in seawater. *Journal of Marine Systems*, *5*(2), 111–118. https://doi.org/10.1016/0924-7963(94)90026-4

Friedlingstein, P., Dufresne, J.-L., Cox, P. M., & Rayner, P. (2003). How positive is the feedback between climate change and the carbon cycle? *Tellus B: Chemical and Physical Meteorology*, *55*(2), 692–700. https://doi.org/10.1034/j.1600-0889.2003.01461.x

Friedlingstein, P., O'Sullivan, M., Jones, M. W., Andrew, R. M., Hauck, J., Olsen, A., et al. (2020). Global carbon budget 2020. *Earth System Science Data*, *12*(4), 3269–3340. https://doi.org/10.5194/essd-12-3269-2020

Gallego, M. A., Timmermann, A., Friedrich, T., & Zeebe, R. E. (2018). Drivers of future seasonal cycle changes in oceanic pCO_2. *Biogeosciences*, *15*(17), 5315–5327. https://doi.org/10.5194/bg-15-5315-2018

Goodwin, P., Williams, R. G., Roussenov, V. M., & Katavouta, A. (2019). Climate sensitivity from both physical and carbon cycle feedbacks. *Geophysical Research Letters*, *46*(13), 7554–7564. https://doi.org/10.1029/2019GL082887

Gorgues, T., Aumont, O., & Rodgers, K. B. (2010). A mechanistic account of increasing seasonal variations in the rate of ocean uptake of anthropogenic carbon. *Biogeosciences*, *7*(8), 2581–2589. https://doi.org/10.5194/bg-7-2581-2010

Goris, N., Tjiputra, J. F., Olsen, A., Schwinger, J., Lauvset, S. K., & Jeansson, E. (2018). Constraining projection-based estimates of the future North Atlantic carbon uptake. *Journal of Climate*, *31*(10), 3959–3978. https://doi.org/10.1175/JCLI-D-17-0564.1

Gruber, N., Clement, D., Carter, B. R., Feely, R. A., vanHeuven, S., Hoppema, M., et al. (2019). The oceanic sink for anthropogenic CO_2 from 1994 to 2007. *Science*, *363*(6432), 1193–1199. https://doi.org/10.1126/science.aau5153

Hagens, M., & Middelburg, J. J. (2016). Attributing seasonal pH variability in surface ocean waters to governing factors. *Geophysical Research Letters*, *43*(24), 12528–12537. https://doi.org/10.1002/2016GL071719

Hauck, J., & Völker, C. (2015). Rising atmospheric CO 2 leads to large impact of biology on Southern ocean CO 2 uptake via changes of the Revelle factor. *Geophysical Research Letters*, *42*(5), 1459–1464. https://doi.org/10.1002/2015GL063070

Hauck, J., Völker, C., Wolf-Gladrow, D. A., Laufkötter, C., Vogt, M., Aumont, O., et al. (2015). On the Southern Ocean CO_2 uptake and the role of the biological carbon pump in the 21st century. *Global Biogeochemical Cycles*, *29*(9), 1451–1470. https://doi.org/10.1002/2015GB005140

Jones, C. D., & Friedlingstein, P. (2020). Quantifying process-level uncertainty contributions to TCRE and carbon budgets for meeting Paris Agreement climate targets. *Environmental Research Letters*, *15*(7), 074019. https://doi.org/10.1088/1748-9326/ab858a

Katavouta, A., Williams, R. G., Goodwin, P., & Roussenov, V. (2018). Reconciling atmospheric and oceanic views of the transient climate response to emissions. *Geophysical Research Letters*, *45*(12), 6205–6214. https://doi.org/10.1029/2018GL077849

Kessler, A., & Tjiputra, J. (2016). The Southern Ocean as a constraint to reduce uncertainty in future ocean carbon sinks. *Earth System Dynamics*, *7*(2), 295–312. https://doi.org/10.5194/esd-7-295-2016

Khatiwala, S., Tanhua, T., Mikaloff Fletcher, S., Gerber, M., Doney, S. C., Graven, H. D., et al. (2013). Global ocean storage of anthropogenic carbon. *Biogeosciences*, *10*(4), 2169–2191. https://doi.org/10.5194/bg-10-2169-2013

Kwiatkowski, L., & Orr, J. C. (2018). Diverging seasonal extremes for ocean acidification during the twenty-first century. *Nature Climate Change*, *8*(2), 141–145. https://doi.org/10.1038/s41558-017-0054-0

Landschützer, P., Gruber, N., Bakker, D. C. E., Stemmler, I., & Six, K. D. (2018). Strengthening seasonal marine CO_2 variations due to increasing atmospheric CO_2. *Nature Climate Change*, *8*(2), 146–150. https://doi.org/10.1038/s41558-017-0057-x

Lewis, E., & Wallace, D. W. R. (1998). *Program developed for CO_2 system calculations*. ORNL/CDIAC-105 (p. 4735). Carbon Dioxide Information Analysis Center, Oak Ridge National Laboratory, U.S. Department of Energy, Oak Ridge, Tennessee. Environmental Sciences Division. Publication No. 4735.

McNeil, B. I., & Sasse, T. P. (2016). Future ocean hypercapnia driven by anthropogenic amplification of the natural CO_2 cycle. *Nature*, *529*(7586), 383–386. https://doi.org/10.1038/nature16156

Mehrbach, C., Culberson, C. H., Hawley, J. E., & Pytkowicx, R. M. (1973). Measurement of the apparent dissociation constants of carbonic acid in seawater at atmospheric pressure. *Limnology & Oceanography*, *18*(6), 897–907. https://doi.org/10.4319/lo.1973.18.6.0897

Middelburg, J. J., Soetaert, K., & Hagens, M. (2020). Ocean alkalinity, buffering and biogeochemical processes. *Reviews of Geophysics*, *58*(3). https://doi.org/10.1029/2019RG000681

Mongwe, N. P., Vichi, M., & Monteiro, P. M. S. (2018). The seasonal cycle of pCO_2 and CO_2 fluxes in the Southern Ocean: Diagnosing anomalies in CMIP5 Earth system models. *Biogeosciences*, *15*(9), 2851–2872. https://doi.org/10.5194/bg-15-2851-2018

Nevison, C. D., Manizza, M., Keeling, R. F., Stephens, B. B., Bent, J. D., Dunne, J., et al. (2016). Evaluating CMIP5 ocean biogeochemistry and Southern Ocean carbon uptake using atmospheric potential oxygen: Present-day performance and future projection. *Geophysical Research Letters*, *43*(5), 2077–2085. https://doi.org/10.1002/2015GL067584

Omta, A. W., Goodwin, P., & Follows, M. J. (2010). Multiple regimes of air-sea carbon partitioning identified from constant-alkalinity buffer factors. *Global Biogeochemical Cycles*, *24*(3). https://doi.org/10.1029/2009GB003726

Orr, J. C. (2011). Recent and future changes in ocean carbonate chemistry. In J.-P. Gattuso, & L. Hansson (Eds.), *Ocean acidification* (pp. 41–66). Oxford University Press.

Orr, J. C., Fabry, V. J., Aumont, O., Bopp, L., Doney, S. C., Feely, R. A., et al. (2005). Anthropogenic ocean acidification over the twenty-first century and its impact on calcifying organisms. *Nature*, *437*(7059), 681–686. https://doi.org/10.1038/nature04095

Pilcher, D. J., Brody, S. R., Johnson, L., & Bronselaer, B. (2015). Assessing the abilities of CMIP5 models to represent the seasonal cycle of surface ocean pCO_2. *Journal of Geophysical Research: Oceans*, *120*(7), 4625–4637. https://doi.org/10.1002/2015JC010759

Pörtner, H. (2008). Ecosystem effects of ocean acidification in times of ocean warming: A physiologist's view. *Marine Ecology Progress Series*, *373*, 203–217. https://doi.org/10.3354/meps07768

Revelle, R., & Suess, H. E. (1957). Carbon dioxide exchange between atmosphere and ocean and the question of an increase of atmospheric CO_2 during the past decades. *Tellus*, *9*(1), 18–27. https://doi.org/10.1111/j.2153-3490.1957.tb01849.x

Riebesell, U., Körtzinger, A., & Oschlies, A. (2009). Sensitivities of marine carbon fluxes to ocean change. *Proceedings of the National Academy of Sciences*, *106*(49), 20602–20609. https://doi.org/10.1073/pnas.0813291106

Rodgers, K. B., Lin, J., & Frölicher, T. L. (2015). Emergence of multiple ocean ecosystem drivers in a large ensemble suite with an Earth system model. *Biogeosciences*, *12*(11), 3301–3320. https://doi.org/10.5194/bg-12-3301-2015

Rodgers, K. B., Sarmiento, J. L., Aumont, O., Crevoisier, C., de Boyer Montégut, C., & Metzl, N. (2008). A wintertime uptake window for anthropogenic CO_2 in the North Pacific. *Global Biogeochemical Cycles*, *22*(2). https://doi.org/10.1029/2006GB002920

Rodgers, K. B., Schlunegger, S., Slater, R. D., Ishii, M., Frölicher, T. L., Toyama, K., et al. (2020). Reemergence of anthropogenic carbon into the ocean's mixed layer strongly amplifies transient climate sensitivity. *Geophysical Research Letters*, *47*(18), 1–9. https://doi.org/10.1029/2020GL089275

Schwinger, J., Tjiputra, J. F., Heinze, C., Bopp, L., Christian, J. R., Gehlen, M., et al. (2014). Nonlinearity of ocean carbon cycle feedbacks in CMIP5 Earth system models. *Journal of Climate*, *27*(11), 3869–3888. https://doi.org/10.1175/JCLI-D-13-00452.1

Sundquist, E. T., Plummer, L. N. L., & Wigley, T. M. L. (1979). Carbon dioxide in the ocean surface: The homogeneous buffer factor. *Science*, *204*(4398), 1203–1205. https://doi.org/10.1126/science.204.4398.1203

Takahashi, T., Olafsson, J., Goddard, J. G., Chipman, D. W., & Sutherland, S. C. (1993). Seasonal variation of CO_2 and nutrients in the high-latitude surface oceans: A comparative study. *Global Biogeochemical Cycles*, *7*(4), 843–878. https://doi.org/10.1029/93GB02263

Takahashi, T., Sutherland, S. C., Sweeney, C., Poisson, A., Metzl, N., Tilbrook, B., et al. (2002). Global sea–air CO_2 flux based on climatological surface ocean pCO_2, and seasonal biological and temperature effects. *Deep Sea Research Part II: Topical Studies in Oceanography*, *49*(9–10), 1601–1622. https://doi.org/10.1016/S0967-0645(02)00003-6

Thyng, K., Greene, C., Hetland, R., Zimmerle, H., & DiMarco, S. (2016). True colors of oceanography: Guidelines for effective and accurate colormap selection. *Oceanography*, *29*(3), 9–13. https://doi.org/10.5670/oceanog.2016.66

Tokarska, K. B., Stolpe, M. B., Sippel, S., Fischer, E. M., Smith, C. J., Lehner, F., & Knutti, R. (2020). Past warming trend constrains future warming in CMIP6 models. *Science Advances*, *6*(12), 1–14. https://doi.org/10.1126/sciadv.aaz9549

Uppström, L. R. (1974). The boron-chlorinity ratio of deep seawater from the Pacific Ocean. *Deep-Sea Research Part I*, *21*(2), 161–162. https://doi.org/10.1016/0011-7471(74)90074-6

van Heuven, S. M. A. C., Pierrot, D., Rae, J. W. B., Lewis, E., & Wallace, D. W. R. (2011). *MATLAB program developed for CO_2 system calculations*. ORNL/CDIAC-105b. Carbon Dioxide Information Analysis Center, Oak Ridge National Laboratory, U.S. Department of Energy. https://doi.org/10.3334/CDIAC/otg.CO2SYS_MATLAB_v1.1

Weiss, R. (1974). Carbon dioxide in water and seawater: The solubility of a non-ideal gas. *Marine Chemistry*, *2*(3), 203–215. https://doi.org/10.1016/0304-4203(74)90015-2